



Development of low-temperature sintered Mn–Co spinel coatings on Fe–Cr ferritic alloys for solid oxide fuel cell interconnect applications

Ding Rong Ou^{a,*}, Mojie Cheng^a, Xiu-Ling Wang^{a,b}

^a Division of Fuel Cells and Battery, Dalian National Laboratory for Clean Energy, Dalian Institute of Chemical Physics, Chinese Academy of Sciences, 457 Zhongshan Road, Dalian 116023, China

^b Graduate University of Chinese Academy of Sciences, Beijing, 100039, China

HIGHLIGHTS

- We develop a low-temperature sintered coating for SOFC metallic interconnects.
- The bicomponent coating material $\text{MnCo}_2\text{O}_4\text{--MnO}_2$ can be air sintered at 800 °C.
- $\text{MnCo}_2\text{O}_4\text{--MnO}_2$ coating greatly improves the oxidation resistance of SUS430 alloy.
- $\text{MnCo}_2\text{O}_4\text{--MnO}_2$ coating is well conductive and stable during long-term oxidation.
- Cr exhaustion of SUS430 alloy is inhibited by $\text{MnCo}_2\text{O}_4\text{--MnO}_2$ coating.

ARTICLE INFO

Article history:

Received 31 October 2012

Received in revised form

17 February 2013

Accepted 20 February 2013

Available online 28 February 2013

Keywords:

Low-temperature sintering

Protective coatings

Spinel oxides

Metallic interconnects

Solid oxide fuel cells

ABSTRACT

To reduce the sintering temperature of spinel coatings to a safe temperature for Fe–Cr ferritic alloys, an $\text{MnCo}_2\text{O}_4\text{--MnO}_2$ bicomponent coating has been prepared on SUS430 ferritic alloy by slurry coating, followed by air sintering at a temperature of 800 °C. The resultant coating is stable during cyclic oxidation tests and is effective at improving the oxidation resistance of SUS430 alloy. The area-specific resistance of coated samples remains nearly constant during long-term oxidation at 800 °C and is less than 6 mΩ cm² even after oxidation for 1000 h. These results indicate that the low-temperature sintered $\text{MnCo}_2\text{O}_4\text{--MnO}_2$ coating is a promising protective material for Fe–Cr ferrite alloys, especially SUS430, which are seriously oxidized at temperatures ≥ 850 °C.

© 2013 Elsevier B.V. All rights reserved.

1. Introduction

Solid oxide fuel cells (SOFCs) are highly promising devices that can convert chemical energy into electrical energy with an electrical efficiency of up to 60%. They can directly use purified coal gas and natural gas as fuels. Therefore, this technology has been considered an important tool for improving the energy utilization of fossil fuels while reducing pollutant emission. Nevertheless, high cost is still a major obstacle to the commercialization of SOFC technology. For this reason, the development of cheaper materials and simpler manufacturing processes for SOFC devices is urgently needed.

* Corresponding author. Tel.: +86 411 84379028(O).

E-mail address: oudingrong@dicp.ac.cn (D.R. Ou).

In recent years, due to the reduction of operating temperatures to below 850 °C, Fe–Cr ferritic alloys, e.g., type 430 alloy, ZMG 232 L and Croffer22 APU alloys, have been studied as interconnect materials for SOFCs [1–8]. Because they are less expensive than ceramic interconnects and exhibit good workability, metallic interconnects could reduce the cost of SOFCs. To restrain the thickening of oxide scale during long-term operation and therefore the increase in area-specific electrical resistance (ASR), a protective coating is usually applied on the surface of metallic interconnects, which is particularly important for type 430 alloys that possess a low Cr content. Moreover, an effective coating could prevent Cr evaporation and the poisoning of cathode materials.

Currently, the most promising coating material for Fe–Cr ferritic alloys is Mn–Co spinel oxides, which have a high electronic conductivity at the operating temperature of SOFCs and a thermal expansion coefficient (TEC) that matches that of ferric alloys [9–14].

Table 1
Chemical composition of the ferritic alloy SUS430 (in wt.%).

	C	Cr	Mn	Si	Ni	S	P	Fe
SUS430	0.04	16.36	0.24	0.37	0.09	0.001	0.016	Balance

A common method for preparing a spinel protective layer on metallic interconnects is slurry coating. However, the green coatings of Mn–Co spinel oxides are difficult to densify at a temperature lower than 1000 °C [15]. Air sintering at a high temperature (~ 1000 °C) may fatally damage thin 430 alloy interconnects. Even for ZMG232L, Croffer22 APU and other ferritic alloys containing 20–30 wt.% Cr, a high sintering temperature may promote the growth of oxide scale beneath the protective coating and change the microstructure of the alloy (thereby the mechanical performance). A protective atmosphere during high-temperature sintering could restrain the oxidation during sintering, but the influence of high temperature on the microstructure and mechanical performance of the alloy still exists. For these reasons, it is significantly important to reduce the sintering temperature of Mn–Co spinel coatings to a safer temperature for Fe–Cr alloys (i.e., ≤ 850 °C). A common method is to reduce the spinel coatings before sintering [16,17] or use reduced oxide powders to prepare the slurry [18,19]. Through reduction, metallic cobalt and manganese oxides with lower valence states can form. Then, the reduction products can be oxidized during the following air sintering and facilitate the densification of the protective coatings. However, the reduction process makes the coating preparation process complicated and greatly increases the manufacturing cost of SOFCs.

In the present study, a simple but effective approach of using a bicomponent coating material MnCo_2O_4 – MnO_2 was applied to reduce the sintering temperature of spinel coatings for metallic interconnects. By using a mixture of MnCo_2O_4 and MnO_2 powders for the slurry, the sintering temperature of the protective coating could be reduced to 800 °C. The effects of low-temperature sintered MnCo_2O_4 – MnO_2 coatings on the oxidation resistance, area-specific electrical resistance (ASR) and long-term durability of Fe–Cr ferritic alloys were systemically investigated.

2. Experimental

2.1. Specimen preparation

The ferritic alloy examined was SUS430, a commercial product of Shanxi Taiyuan Stainless Steel Co., LTD. The chemical composition of the alloy is listed in Table 1. Rectangular specimens measuring 20 mm \times 20 mm were cut from a 2 mm thick steel sheet. Then, the plates were ground with SiC abrasive paper of #320–#1000 and then cleaned in an ultrasonic ethanol bath.

In the present study, the slurry coating technique was applied to prepare oxide layers on the SUS430 plates. The preparation process for the protective coatings is illustrated in Fig. 1. Before coating, all of the plates were pre-oxidized at 800 °C for 25 h to form a thin oxide scale (~ 0.5 μm in the present study) on the alloy and thereby increase the adhesion of the oxide coating to the metal substrate. MnCo_2O_4 powder was synthesized by solid-state synthesis using commercial MnO_2 and Co_3O_4 powders as source materials. A slurry consisting of the mixture of MnCo_2O_4 and MnO_2 powders, PVB and ethanol was prepared and applied to the pre-oxidized plates by

dip-coating. In this study, the mole ratio of MnCo_2O_4 and MnO_2 was set to 1:0.5. Then, the green coating was dried and sintered at 800 °C for 8–50 h. For comparison, a MnCo_2O_4 coating was also applied to pre-oxidized SUS430 by slurry coating and air sintered at 800 °C.

2.2. Measurements and characterizations

The oxidation kinetics of bare and coated steel plates was investigated by performing cyclic oxidation tests in ambient air. In a test cycle, the plates were heated to 800 °C at 5 °C min^{-1} , held at that temperature for 25–50 h and then cooled to room temperature. The oxidation weight gain of each plate was measured after every cyclic test. Usually, the high-temperature oxidation of Fe–Cr alloy is controlled by solid-state diffusion through the oxide scale, and the oxidation weight gain follows a parabolic law:

$$\Delta w^2 = k_p t + c, \quad (1)$$

where Δw^2 is the weight gain squared, k_p is the parabolic fit constant, t is the period during which the alloy is held at the designed temperature, and c is a constant that accounts for the scale present before the isothermal exposure [5,6]. From the measured values of weight gain as a function of holding time at 800 °C, the constant k_p was calculated according to Eq. (1).

The electrical resistance of bare and coated plates was measured by a four-probe DC technique using Au electrodes. Measurements were taken at intervals of 50 °C from 800 °C to 400 °C. After the alloy was held at the designed temperature for 30–60 min for stabilization, measurements were performed in air. Then, the ASRs (expressed in $\text{m}\Omega \text{ cm}^2$) of the scales and coatings were calculated according to Ohm's law, $\text{ASR} = AU/2I$, where A is the sample area, U is the voltage drop and I is the electric current. A factor of 2 was included to account for the fact that the voltage drop was measured across two oxide scales or coatings connected in series. Then, the activation energy (E_a) for electric conduction was estimated by using the equation

$$T/\text{ASR} = k_1 \exp(-E_a/RT), \quad (2)$$

where T is the measurement temperature and k_1 is a constant that depends only on sample properties.

The crystal structures of the oxide scales and coatings were analyzed by X-ray diffraction (XRD) using a Rigaku D/Max2500VB2 X-ray Generator with Cu K α radiation. The diffraction peaks were identified according to the lattice constants indicated by JCPDS cards [20]. Microstructural and compositional characterizations were performed using an FEI scanning electron microscope (SEM, model Quanta 200FEG) equipped with an energy-dispersive X-ray spectroscopy (EDX) instrument. After analyzing the surface, sample cross-sections were prepared by epoxy-mounting and polishing and further examined by SEM.

To investigate the TEC and electric conductivity of the coating materials, rectangular bulk samples of MnCo_2O_4 and MnCo_2O_4 – MnO_2 were prepared and sintered at 1200 °C for 2 h. The size of the bulk samples is 2 mm \times 5 mm \times 25 mm. Then, the TEC was measured using a NETZSCH DIL 402C dilatometer from room temperature to 850 °C. The electric conductivity σ of the bulk specimens was measured by the four-probe DC technique using Ag

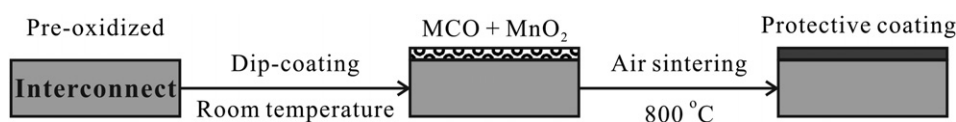


Fig. 1. Schematic of the preparation of MnCo_2O_4 – MnO_2 coatings on metallic interconnects by slurry coating. MCO: $(\text{Mn, Co})_3\text{O}_4$ spinel oxides.

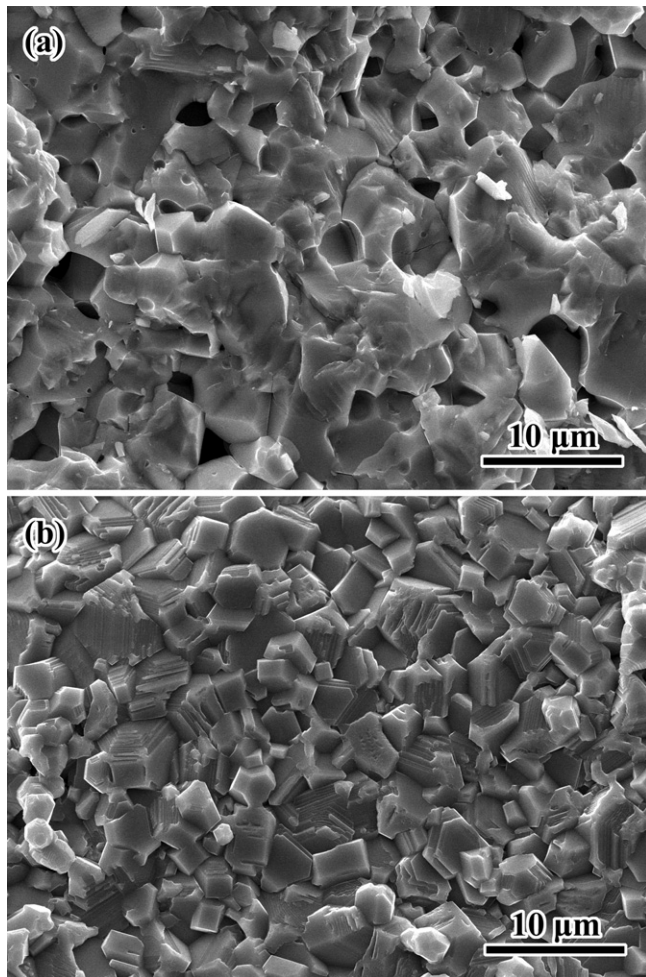


Fig. 2. SEM images of the fracture surface of MnCo_2O_4 and $\text{MnCo}_2\text{O}_4\text{-MnO}_2$ bulk samples.

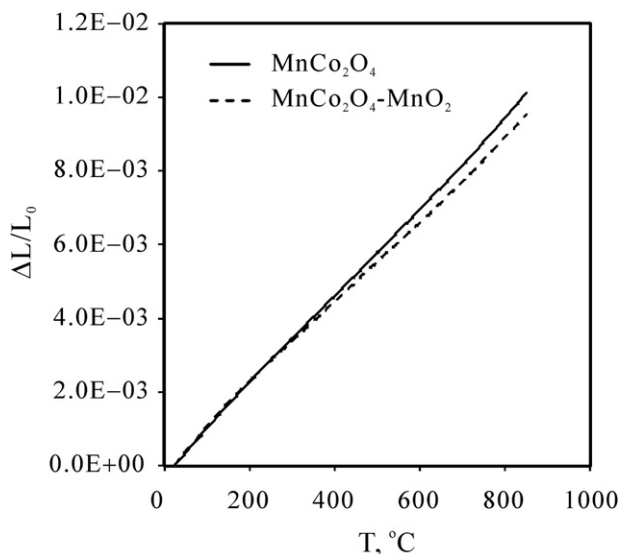


Fig. 3. Thermal expansion of MnCo_2O_4 and $\text{MnCo}_2\text{O}_4\text{-MnO}_2$ bulk samples measured from room temperature to 850 °C.

electrodes. The activation energy of the bulk samples was calculated according to the equation

$$\sigma T = k_2 \exp(-E_a/RT), \quad (3)$$

where k_2 is also a constant that depends on sample properties.

3. Results and discussion

3.1. Properties of $\text{MnCo}_2\text{O}_4\text{-MnO}_2$ oxides

Fig. 2 shows a comparison between the fracture surface of MnCo_2O_4 and $\text{MnCo}_2\text{O}_4\text{-MnO}_2$ bulk samples. It is clearly seen that a considerable amount of small pores exist in the MnCo_2O_4 sample after sintering at 1200 °C. In contrast, the $\text{MnCo}_2\text{O}_4\text{-MnO}_2$ sample is almost fully dense, indicating that the addition of MnO_2 could promote the densification of Mn–Co spinel oxides.

To examine whether $\text{MnCo}_2\text{O}_4\text{-MnO}_2$ can be used as a conductive coating material for Fe–Cr ferritic alloys, the TEC and electrical conductivity of $\text{MnCo}_2\text{O}_4\text{-MnO}_2$ were measured and compared with those of MnCo_2O_4 spinel. Fig. 3 shows the thermal expansion curve of bulk samples $\text{MnCo}_2\text{O}_4\text{-MnO}_2$ and MnCo_2O_4 , from which the TECs of the samples were calculated. Over the temperature range of 30–800 °C, the TECs of $\text{MnCo}_2\text{O}_4\text{-MnO}_2$ and MnCo_2O_4 are $11.6 \times 10^{-6} \text{ K}^{-1}$ and $12.3 \times 10^{-6} \text{ K}^{-1}$, respectively, very close to the TEC of Fe–Cr ferrite alloys ($\sim 12 \times 10^{-6} \text{ K}^{-1}$). Fig. 4 shows Arrhenius plots of both samples, in which the conductivity has not been corrected according to the density. The electrical conductivity of $\text{MnCo}_2\text{O}_4\text{-MnO}_2$ is approximately $\sim 53 \text{ S cm}^{-1}$ at 800 °C, much higher than that of the MnCo_2O_4 specimen ($\sim 34 \text{ S cm}^{-1}$). The matching of the TECs and the high conductivity indicate that $\text{MnCo}_2\text{O}_4\text{-MnO}_2$ oxides with the designed composition could be high-performance coating materials for metallic interconnects composed of Fe–Cr ferritic alloy. Furthermore, the activation energy for electric conduction of the $\text{MnCo}_2\text{O}_4\text{-MnO}_2$ sample is 45 kJ mol^{-1} , which is slightly lower than that of MnCo_2O_4 (50 kJ mol^{-1}). This indicates that the higher conductivity of $\text{MnCo}_2\text{O}_4\text{-MnO}_2$ could be attributed to not only the higher density of the sample (Fig. 2) but also the improved electrical properties of the spinel oxide.

3.2. Microstructure of the low-temperature sintered coatings

In this study, both MnCo_2O_4 and $\text{MnCo}_2\text{O}_4\text{-MnO}_2$ protective coatings on SUS430 were prepared by dip-coating, followed by air sintering at 800 °C. Fig. 5(a) and 5(b) show SEM images of the MnCo_2O_4 and $\text{MnCo}_2\text{O}_4\text{-MnO}_2$ coatings after sintering. As mentioned before, the densification temperature for MnCo_2O_4 is usually above 1000 °C. Therefore, the MnCo_2O_4 coatings sintered at 800 °C were difficult to densify, and a large area of the oxide layer peeled off after sintering (as indicated by arrows in Fig. 5(a)). In contrast, the oxide particles in the $\text{MnCo}_2\text{O}_4\text{-MnO}_2$ coating were well sintered, and a continuous protective layer formed on the alloy surface (Fig. 5(b)). Fig. 5(c) shows the $\text{MnCo}_2\text{O}_4\text{-MnO}_2$ coating after 20 thermal cycles between room temperature and 800 °C (totally holding at 800 °C for 1000 h). It can be seen that the $\text{MnCo}_2\text{O}_4\text{-MnO}_2$ coatings did not chip, crack or separate from the substrate, highlighting the good adhesion among particles in the coating and perfect bonding between the coating and the substrate.

Fig. 6 shows a cross-sectional view of the $\text{MnCo}_2\text{O}_4\text{-MnO}_2$ coating after heating at 800 °C for 1000 h (through 20 thermal cycles). As seen, the low-temperature sintered $\text{MnCo}_2\text{O}_4\text{-MnO}_2$ coating is approximately 15 μm thick. The EDX line-scan profile shows a gradient change of elements at the interface between the coating and the alloy. This interfacial region is labeled in Fig. 6, of which the thickness is only about 1 μm. Because the interfacial

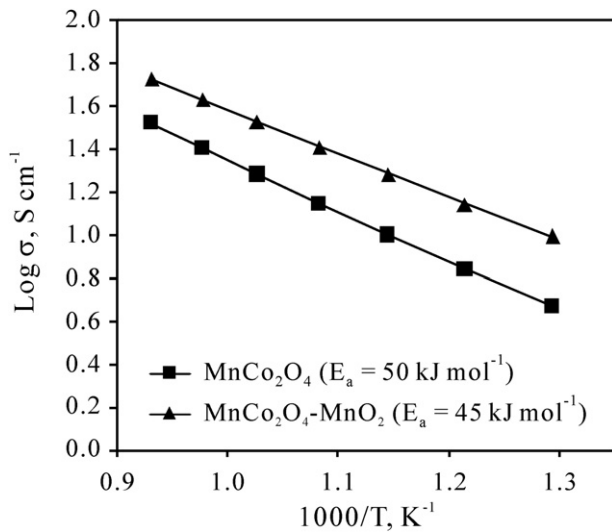


Fig. 4. Arrhenius plots of MnCo_2O_4 and $\text{MnCo}_2\text{O}_4\text{-MnO}_2$ bulk samples. The activation energy calculated is also given in the figure.

region simultaneously contains Mn, Co and Cr, we suspect that it could be the result of a solid-state reaction and/or diffusion between the pre-oxidized substrate and the $\text{MnCo}_2\text{O}_4\text{-MnO}_2$ coating. However, there is no obvious chromium oxide layer between the alloy and the coating, implying that the high-temperature oxidation of the metallic substrate was greatly inhibited by the low-temperature sintered $\text{MnCo}_2\text{O}_4\text{-MnO}_2$ coating. Furthermore, the EDX line-scan profiles show that the Cr content in the coating is low and there is no Cr enrichment on the coating surface. These results indicate that the $\text{MnCo}_2\text{O}_4\text{-MnO}_2$ coating can effectively restrain Cr migration from the alloy.

To identify the crystal structure of the coatings before and after cyclic oxidation, XRD analysis was performed. As shown in Fig. 7, due to the solid-state reaction between MnO_2 and MnCo_2O_4 , the protective coating is dominated by a spinel structure and only a small amount of manganese oxide remained after sintering. The remaining manganese oxide exists as Mn_2O_3 in the coating because it is more stable than MnO_2 under the sintering conditions [14]. Furthermore, diffraction peaks belonging to spinel oxides are slightly shifted to lower angle. These results indicate that the densification of the coating could be due to the solid-state reaction between MnO_2 and MnCo_2O_4 during sintering, and due to the dissolution of Mn oxide into MnCo_2O_4 , the lattice constant of the spinel oxides slightly increased. After heating at 800 °C for 1000 h, nearly all of the manganese oxide in the coating was depleted and the protective coating was dominated by $(\text{Mn},\text{Co})_3\text{O}_4$

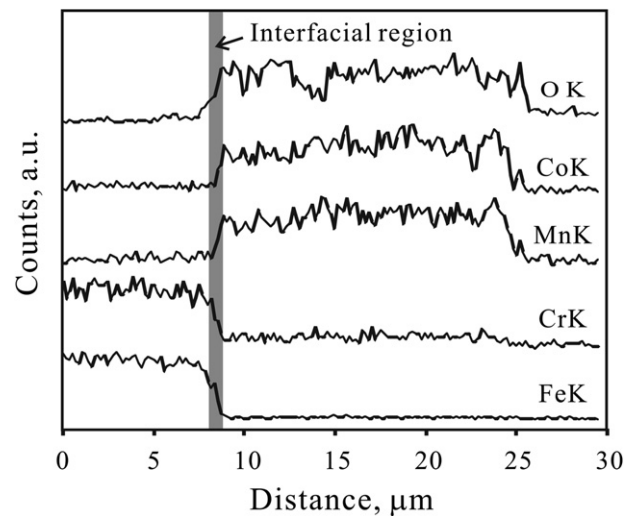
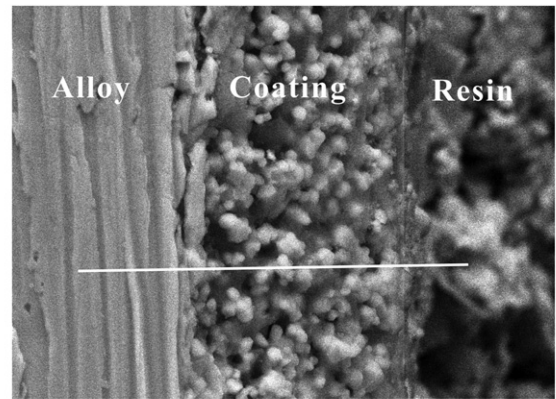


Fig. 6. Cross-sectional SEM image and EDX line-scan profile of $\text{MnCo}_2\text{O}_4\text{-MnO}_2$ -coated plate after cyclic oxidation (holding at 800 °C for 1000 h).

solid solutions. It is expected that the mean atomic ratio of $[\text{Mn}]/[\text{Co}]$ in the resultant solid solutions should approach the average composition of the original $\text{MnCo}_2\text{O}_4\text{-MnO}_2$ coating, i.e., $[\text{Mn}]/[\text{Co}] \sim 0.75$.

3.3. Performance of $\text{MnCo}_2\text{O}_4\text{-MnO}_2$ coatings

One of the important requirements for SOFC metallic interconnects is good oxidation resistance at the operating temperature of the fuel cells. To compare oxide scale growth rates between coated and bare samples, the weight gain per unit area (mg cm^{-2}) was measured after each oxidation test.

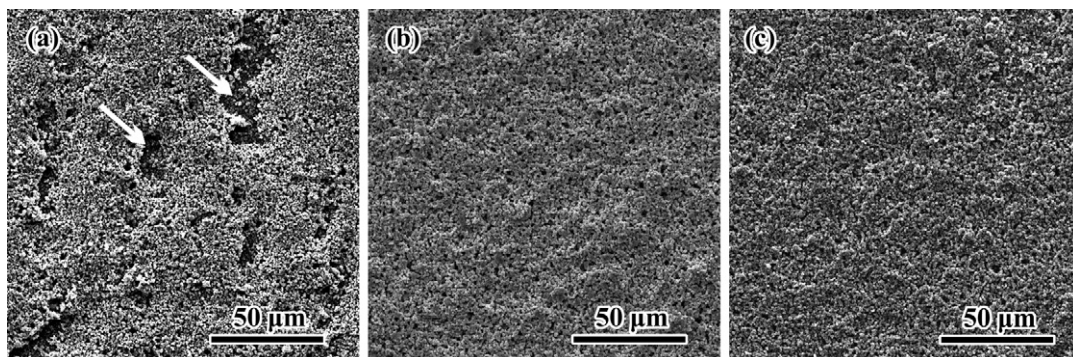


Fig. 5. SEM images of (a) MnCo_2O_4 coating after sintering, (b) $\text{MnCo}_2\text{O}_4\text{-MnO}_2$ coating after sintering and (c) $\text{MnCo}_2\text{O}_4\text{-MnO}_2$ coating after cyclic oxidation (while holding at 800 °C for 1000 h).

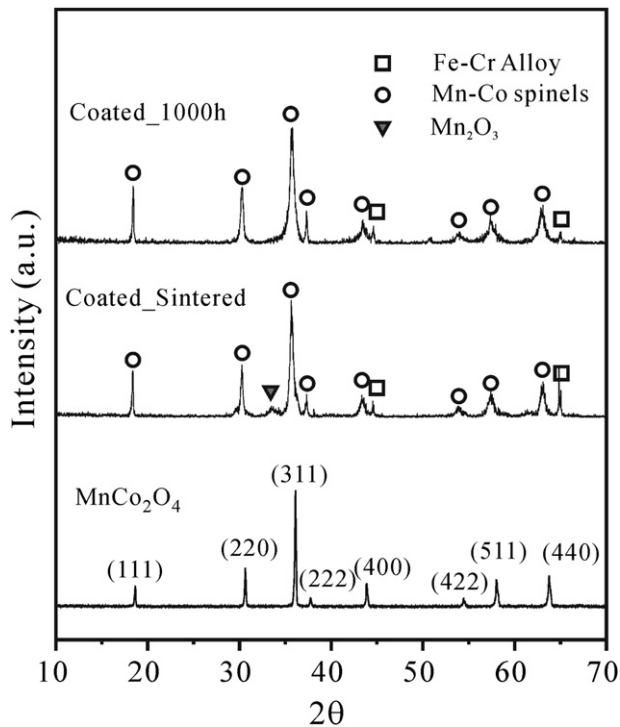


Fig. 7. XRD profiles of the MnCo_2O_4 – MnO_2 -coated SUS430 plates. The diffraction of MnCo_2O_4 powder is also given for comparison.

Fig. 8 shows the squared weight gains of bare and MnCo_2O_4 – MnO_2 -coated SUS430 as a function of heating time at 800 °C. During the oxidation test, the squared weight gain of the bare sample increased linearly with time and two stages of the high-temperature oxidation of bare SUS430 could be observed. The parabolic fit constant k_p calculated according to Eq. (1) was $2.2 \times 10^{-4} \text{ mg}^2 \text{ cm}^{-4} \text{ h}^{-1}$ in the first stage (0–100 h) and decreased to approximately $7.0 \times 10^{-5} \text{ mg}^2 \text{ cm}^{-4} \text{ h}^{-1}$ in the second stage (100–400 h). After 400 h of oxidation, the oxide scale formed on the alloy surface flaked off locally, which led to obvious fluctuations in the curve. Fig. 9 shows the XRD profiles of bare SUS430 plates heated at 800 °C for 100 h and 1000 h. It can be seen that the oxide scale mainly consisted of Cr_2O_3 and Mn–Cr spinel oxides. By increasing the heating time from 100 h to 1000 h, the spinel oxide

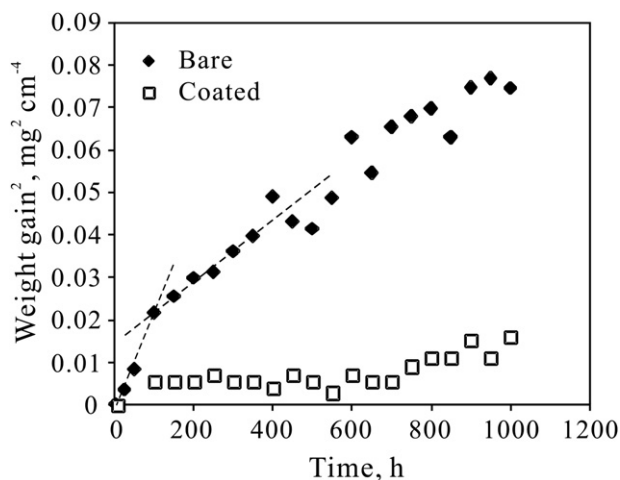


Fig. 8. Squared oxidation weight gain of bare and MnCo_2O_4 – MnO_2 -coated SUS430 as a function of holding time at 800 °C. The measurement error of weight gain is $\pm 0.02 \text{ mg/cm}^2$.

content increased. Therefore, we suspected that the first stage of oxidation, i.e., that exhibiting a higher rate of oxidation, could mainly correspond to the fast growth of Cr_2O_3 , while the formation of spinel oxides could become increasingly dominant in the second stage to slow the oxidation rate of the alloy.

The oxidation behavior observed for the alloy coated with MnCo_2O_4 – MnO_2 was different (Fig. 8). The weight gain increased to 0.07 mg/cm^2 during the first 100 h of oxidation and fluctuated around 0.07 mg/cm^2 from 100 to 700 h, with a measurement error of $\pm 0.02 \text{ mg/cm}^2$. Then it was raised to 0.12 mg/cm^2 during 700–1000 h testing. Furthermore, it can be seen that the weight gain of coated sample is considerable less than that of uncoated sample. Correspondingly, the diffraction of Cr_2O_3 in the XRD profile of the MnCo_2O_4 – MnO_2 -coated samples was too weak to be identified even after heating for 1000 h (as seen in Fig. 7). These results indicate that the oxidation of SUS430 alloy can be effectively inhibited by the low-temperature sintered MnCo_2O_4 – MnO_2 coating.

ASR, another property of metallic interconnects, is significantly important for the power generation performance of SOFCs. Fig. 10(a) displays the ASR curves of bare and coated SUS430 as a function of testing time. Because of the relatively fast oxidation of bare SUS430, the ASR of bare SUS430 measured at 800 °C rapidly approached approximately $400 \text{ m}\Omega \text{ cm}^2$ after heating for 500 h. However, the ASR of the MnCo_2O_4 – MnO_2 -coated plates slightly decreased at the beginning, which could be due to the subtle increase in the density of the coating. Then, the ASR remained low ($\sim 6 \text{ m}\Omega \text{ cm}^2$) until reaching 1000 h of testing. This tendency is well consistent with the weight gain of coated samples shown in Fig. 8 and further demonstrates the excellent oxidation resistance of MnCo_2O_4 – MnO_2 -coated alloy. Furthermore, it can be concluded that the low-temperature sintered MnCo_2O_4 – MnO_2 coating has a high electronic conductivity. Although a small amount of manganese oxide remained in the coatings after low-temperature sintering (Fig. 7), it has no considerable influence on the ASR because the spinel oxide around the manganese oxide particles can form an effective network for electronic conduction.

Fig. 10(b) shows the Arrhenius plots of bare and coated samples, from which the activation energy for electrical conduction was calculated according to Eq. (2). As the oxidation time was increased from 25 h to 500 h, the activation energy of bare SUS430 slightly

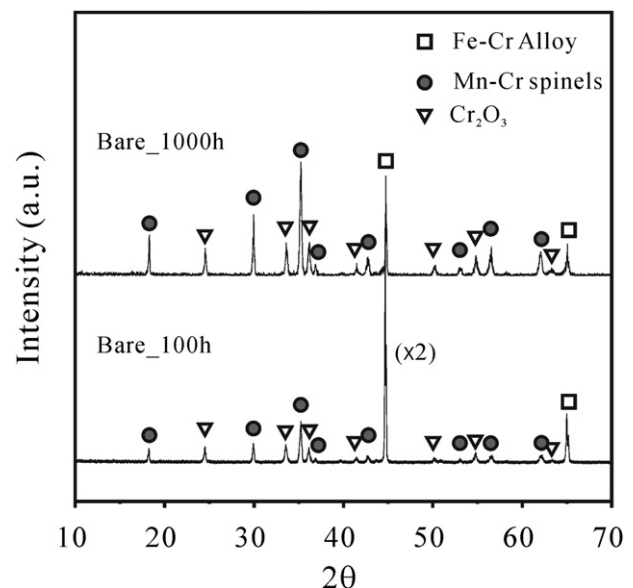


Fig. 9. XRD profiles of bare after oxidation at 800 °C for 100 h and 1000 h.

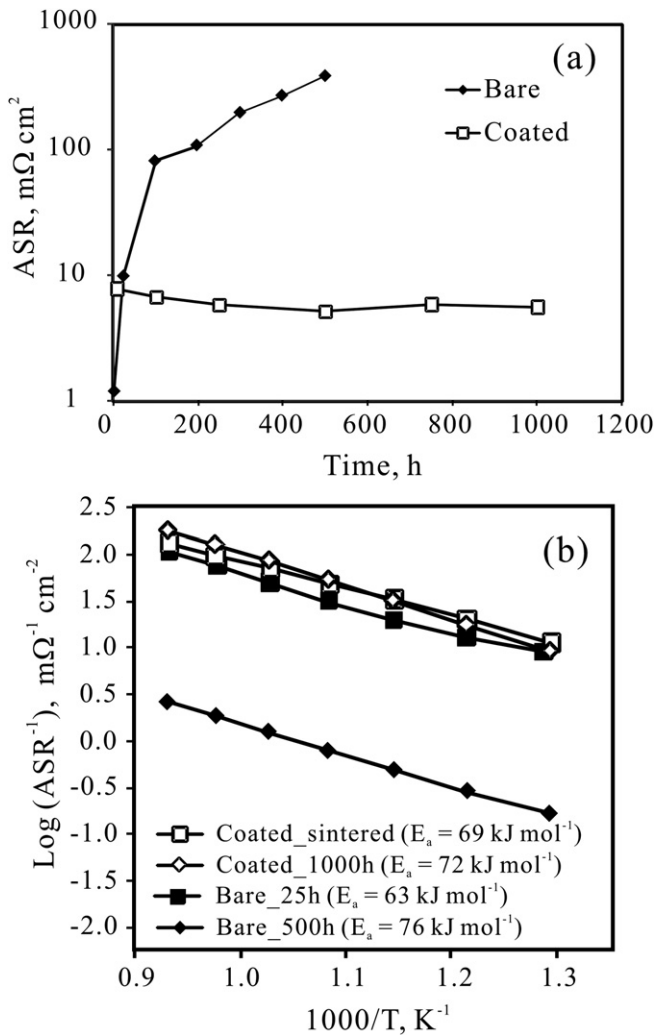


Fig. 10. (a) ASR of bare SUS430 and MnCo_2O_4 – MnO_2 -coated SUS430 alloy measured at 800 °C as a function of holding time at 800 °C. (b) Comparison of Arrhenius plots of bare and coated samples.

increased from 63 kJ mol^{-1} to 72 kJ mol^{-1} . As mentioned before, the oxide scale formed on SUS430 is mainly composed of Mn–Cr spinel and Cr_2O_3 , and the content of Mn–Cr spinel increases with oxidation time (Fig. 9). Because the study of Qu et al. showed that the activation energy of Mn–Cr spinel is much higher than that of Cr_2O_3 [15], it is reasonable to suggest that the increase in the activation energy could be due to the higher content of Mn–Cr spinel after long-term oxidation.

Meanwhile, the activation energy of the sintered coated sample was 69 kJ mol^{-1} , which slightly increased to 76 kJ mol^{-1} after 1000 h of oxidation. These values are much higher than those of the Mn–Co spinel oxides (45 – 50 kJ mol^{-1} , see Fig. 3) but very close to the activation energy of the uncoated sample (63 – 72 kJ mol^{-1}). The values obtained for the activation energy indicate that the electrical behavior of the coated sample is not dominated by the Mn–Co spinel coating. By considering the microstructural features of the coated sample shown in Fig. 6, we suspect that the measured ASR could be mainly attributed to the interfacial layer formed between the coating and the metallic substrate. As shown in Fig. 6, the interfacial layer could be composed of Mn–Cr and/or Mn–Co–Cr spinel oxides. The literature reveals that the conductivities of Cr_2O_3 and Mn–Cr spinel oxides [15] are approximately 2–4 orders of magnitude lower than those of Mn–Co spinel oxides at the measurement

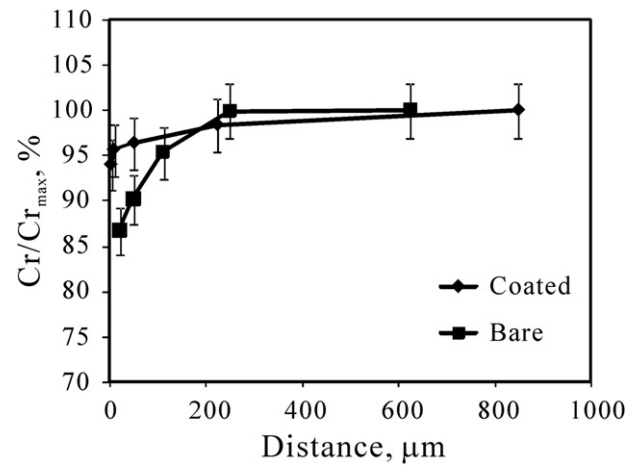


Fig. 11. Relative Cr content of bare and MnCo_2O_4 – MnO_2 -coated SUS430 plates after cyclic oxidation (holding at 800 °C for 1000 h) plotted as a function of distance from the alloy surface.

temperatures employed in this study. Therefore, the contribution of the Cr-rich interfacial layer to the ASR could be much greater than that of the coating though the interfacial layer is thin, which could dominate the conduction behavior of coated samples and leads to the higher activation energy of the coated sample, as shown in Fig. 10(b). This result indicates that, to improve the electrical performance of metallic interconnects, the control of the coating-alloy interface is significantly important.

3.4. Influence on Cr exhaustion

Due to the formation of Cr-containing oxide scale on the alloy surface and the migration of Cr away from the alloys, the Cr content in the alloy is readily reduced, especially in the region near the surface. When the Cr content in the alloy is too low to provide effective protection for the alloy, the destruction of the metallic interconnect may occur [21].

Fig. 11 shows the relative Cr content as a function of distance from the metal surface (i.e., the metal/oxide scale interface of the bare alloy and the metal/coating interface of the coated sample). Both the bare and coated samples were oxidized at 800 °C for 1000 h through 20 thermal cycles. Near the metal surface of bare SUS430, the Cr content drops by 14% of the original value and the thickness of the influencing layer is approximately 0.20–0.25 mm. These results indicate that, during long-term oxidation, the exhaustion of Cr could be a serious problem for uncoated SUS430 interconnects thinner than 0.4–0.5 mm. This conclusion is consistent with that suggested by Uehara et al. [21]. Nevertheless, in the case of the MnCo_2O_4 – MnO_2 -coated sample, the relative decline in the Cr content near the metal/coating interface was only approximately 5%. The effect of the MnCo_2O_4 – MnO_2 coating on Cr exhaustion can be explained by the improved oxidation resistance and restrained Cr migration of the MnCo_2O_4 – MnO_2 -coated alloy. Taking all of the results into account, it is believed that the MnCo_2O_4 – MnO_2 -coated sample could exhibit much better oxidation resistance and stability during long-term operation.

4. Conclusions

High-performance spinel coatings on SUS430 alloy have been successfully synthesized using MnCo_2O_4 – MnO_2 slurry, followed by air sintering at 800 °C. The low-temperature sintered MnCo_2O_4 – MnO_2 coating was highly conductive and could greatly improve the oxidation resistance of alloy SUS430. Furthermore,

the migration of Cr through the coating was subtle, and the exhaustion of Cr exhaustion in the alloy was greatly inhibited. Taking all of the results into account, it was concluded that the low-temperature sintered $\text{MnCo}_2\text{O}_4\text{--MnO}_2$ coating could be a promising protective material for Fe–Cr ferrite alloys, especially for SUS430 alloy, which is seriously oxidized at temperatures above 850 °C.

Acknowledgment

The financial support of the National Natural Science Foundation of China (No. 51101146), the National Basic Research Program of China (No. 2012CB215500 and 2010CB732302), the National High Technology Research and Development program of China (Grant No. 2011AA050704) and the Scientific Research Foundation for the Returned Overseas Chinese Scholars, Satate Education Ministry is gratefully acknowledged.

References

- [1] N. Shaigan, W. Qu, D.G. Ivey, W. Chen, J. Power Sources 195 (2010) 1529–1542.
- [2] Z. Yang, Int. Mater. Rev. 53 (2008) 39–54.
- [3] J.W. Fergus, Mater. Sci. Eng. A 397 (2005) 271–283.
- [4] B. Hua, J. Pu, F. Lu, J. Zhang, B. Chi, L. Jian, J. Power Sources 195 (2010) 2782–2788.
- [5] T. Horita, Y. Xiong, H. Kishimoto, K. Yamaji, N. Sakai, H. Yokokawa, J. Power Sources 131 (2004) 293–298.
- [6] H. Kurokawa, K. Kawamura, T. Maruyama, Solid State Ionics 168 (2004) 13–21.
- [7] I. Antepara, I. Villarreal, L.M. Rodríguez-Martínez, N. Lecanda, U. Castro, A. Laresgoiti, J. Power Sources 151 (2005) 103–107.
- [8] J. Froitzheim, G.H. Meier, L. Niewolak, P.J. Ennis, H. Hatterndorf, L. Singheiser, W.J. Quadackers, J. Power Sources 178 (2008) 163–173.
- [9] T. Uehara, N. Yasuda, M. Okamoto, Y. Baba, J. Power Sources 196 (2011) 7251–7256.
- [10] Z. Yang, G.-G. Xia, C.-M. Wang, Z. Nie, J. Templeton, J.W. Stevenson, P. Singh, J. Power Sources 183 (2008) 660–667.
- [11] Z. Yang, G.-G. Xia, X.-H. Li, J.W. Stevenson, Int. J. Hydrog. Energy 32 (2007) 3648–3654.
- [12] B. Hua, J. Pu, W. Gong, J. Zhang, F. Lu, L. Jian, J. Power Sources 185 (2008) 419–422.
- [13] Z. Yang, G. Xia, Z. Nie, J. Templeton, J.W. Stevenson, Electrochem. Solid State Lett. 11 (2008) B140–B143.
- [14] A. Petric, H. Ling, J. Am. Ceram. Soc. 90 (2007) 1515–1520.
- [15] W. Qu, L. Jian, J.M. Hill, D.G. Ivey, J. Power Sources 153 (2006) 114–124.
- [16] Z. Yang, G. Xia, Z. Nie, J. Templeton, J.W. Stevenson, Electrochem. Solid State Lett. 11 (2005) A168–A170.
- [17] Patent: Y. Baba, H. Kameda, H. Kurokawa, Y. Matsuzaki, K. Ogasawara, S. Yamashita. "Protection Film Coating Method on Interconnector for SOFC" Tokyo Gas Co Ltd, JP2009–152016A.
- [18] X. Xin, S. Wang, Q. Zhu, Y. Xu, T. Wen, Electrochem. Commun. 12 (2010) 40–43.
- [19] X. Xin, S. Wang, J. Qian, C. Lin, Z. Zhan, T. Wen, Int. J. Hydrogen Energy 37 (2012) 471–476.
- [20] JCPDS-International Center for Diffraction Data, Card No. 33–0892 ($\text{Mn}_{1.5}\text{Cr}_{1.5}\text{O}_4$), Card No. 75–1614 (MnCr_2O_4), Card No. 24–1237 (MnCo_2O_4), Card No. 24–0507 (Mn_2O_3), Card No. 38–1479 (Cr_2O_3).
- [21] T. Uehara, N. Yasuda, M. Okamoto, C. Aoki, T. Ohno, A. Toji, ECS Transactions 25 (2009) 1455–1462.